Distinct Nrf2 Signaling Thresholds Mediate Lung Tumor Initiation and Progression

Janine M. DeBlasi[1,2], Aimee Falzone[1], Samantha Caldwell[1], Nicolas Prieto-Farigua[1], Justin R. Prigge[3], Edward E. Schmidt[3], Iok In Christine Chio[4,5], Florian A. Karreth[6], Gina M. DeNicola[1*]

[1]Department of Cancer Physiology, H. Lee Moffitt Cancer Center and Research Institute, Tampa, FL, 33612, USA.
[2]Cancer Biology PhD Program, University of South Florida, Tampa, FL 33612, USA.
[3]Microbiology & Cell Biology Department, Montana State University, Bozeman, MT 59717, USA.
[4]Institute for Cancer Genetics, Department of Genetics and Development, Columbia University Irving Medical Center, New York, NY 10032, USA.
[5]Herbert Irving Comprehensive Cancer Center, Columbia University Irving Medical Center, New York, NY 10032, USA.
[6]Department of Molecular Oncology, H. Lee Moffitt Cancer Center and Research Institute, Tampa, FL, 33612, USA.

*Corresponding author. E-mail: gina.denicola@moffitt.org

Keywords: Nuclear factor erythroid 2-related factor 2 (**NRF2**), Kelch-like ECH-associated protein 1 (**KEAP1**), Non-small cell lung cancer (**NSCLC**), Genetically engineered mouse model (**GEMM**)

Abstract

Mutations in the KEAP1-NRF2 pathway occur in up to a third of non-small cell lung cancer (NSCLC) cases and often confer resistance to therapy and poor outcomes. Here, we developed murine alleles of the KEAP1 and NRF2 mutations found in human NSCLC and comprehensively interrogated their impact on tumor initiation and progression. Chronic Nrf2 stabilization by Keap1 or Nrf2 mutation was not sufficient to induce tumorigenesis, even in the absence of tumor suppressors p53 or Lkb1. When combined with Kras$^{G12D/+}$, constitutive Nrf2 activation promoted lung tumor initiation and early progression of hyperplasia to low-grade tumors but impaired their progression to advanced-grade tumors, which was reversed by Nrf2 deletion. Finally, NRF2 overexpression in KEAP1 mutant NSCLC cell lines was detrimental to cell proliferation, viability, and anchorage-independent colony formation. Collectively, our results

38 establish the context-dependence and activity threshold for NRF2 during the lung
39 tumorigenic process.
40
41 **Main**
42
43 NRF2 (nuclear factor-erythroid 2 p45-related factor 2) is a stress-responsive
44 transcription factor that regulates the detoxification of reactive oxygen species (ROS),
45 maintains cellular homeostasis, and regulates many facets of metabolism[1,2]. NRF2 is
46 negatively regulated by KEAP1 (Kelch-like ECH-associated protein 1), a substrate
47 adaptor protein for the cullin 3 (CUL3)-based E3 ubiquitin ligase that facilitates NRF2
48 ubiquitination and proteasomal degradation in the absence of oxidative or xenobiotic
49 stress[3]. NRF2 promotes the detoxification of carcinogens to limit deleterious mutations
50 that initiate cancer[4-7] and NRF2 activators are being explored as chemopreventative
51 agents[8-10]. However, NRF2 is frequently stabilized in many cancers, particularly non-
52 small cell lung cancer (NSCLC), where mutations in the KEAP1-NRF2 pathway are
53 found in up to 30% of cases[11,12]. NRF2 stabilization is associated with poor prognosis[13-
54 18], resistance to chemo- and radiotherapy[19,20], cancer cell survival[20], proliferation[21],
55 metabolic reprogramming[22-24], and metastasis[25]. It remains unclear, however, whether
56 chronic NRF2 stabilization transforms normal cells. Thus, it is important to understand
57 the contexts and mechanisms by which NRF2 can prevent and promote cancer
58 phenotypes.
59
60 Preclinical genetically engineered mouse models (GEMMs) have advanced our
61 understanding of the role of NRF2 in lung tumorigenesis[21,25-35]. NRF2 activation in
62 NSCLC has been modeled in GEMMs by inactivating Keap1 via conditional knockout[26-
63 29,31,33] or CRISPR-mediated deletion[25,32,34,35], in contrast to the KEAP1 mutations found
64 in human lung cancer. These studies have shown that Nrf2 promotes lung tumor
65 initiation[27,28], tumor size[32,36], progression[31,32], and metastasis[25]. However, other studies
66 have failed to see an effect of Nrf2 on lung tumor initiation[36,37] or size[34,35,37], and we
67 reported that Nrf2 activation significantly decreases tumor size[30]. Study conditions, time
68 points and phenotypes assayed varied across these studies. Therefore, the role NRF2

69 activation plays at distinct stages of tumor initiation and progression remains to be
70 determined.
71
72 In the current study, we generated lung cancer GEMMs expressing Keap1^{R554Q} and
73 Nrf2^{D29H} mutations to comprehensively investigate how Nrf2 activation affects each
74 stage of the tumorigenic process. These models also exhibit a series of graded NRF2
75 activation, allowing us to ask how different levels of Nrf2 influence lung tumor
76 progression. We found that constitutive Nrf2 stabilization induced by these mutations
77 was insufficient for lung tumor development, even in the context of tumor suppressor
78 loss. In contrast, these mutations promoted lung tumor initiation in the Kras$^{G12D/+}$ model
79 of early lung adenocarcinoma, consistent with previous studies[21,27,28].
80 Using the Kras$^{G12D/+}$; p53$^{fl/fl}$ adenocarcinoma model, we found that homozygous Keap1
81 mutation unexpectedly blocked tumor progression. Supportingly, we found that Nrf2
82 expression and activity was downregulated in advanced tumors, and Nrf2 deletion could
83 rescue the Keap1 mutation-mediated progression impairment. Overall, our data suggest
84 that NRF2 has distinct, threshold-dependent effects during lung tumor initiation and
85 progression.
86
87 **Results**
88 ***Keap1^{R554Q}* and *Nfe2l2^{D29H}* alleles activate the Nrf2 transcriptional program**
89 To study the role of NRF2 activation in lung cancer, we developed alleles harboring
90 either the Keap1^{R554Q} or the Nrf2^{D29H} mutation found in human NSCLC **(Fig. 1a, b)**.
91 Both Keap1^{R554Q} and Nrf2^{D29H} mutations prevent Keap1-mediated ubiquitination of Nrf2,
92 allowing for constitutive expression of Nrf2 and transcription of Nrf2 target genes[38,39]. To
93 generate the conditionally active *(CA)-Keap1^{R554Q}* allele, we inserted a wild-type *Keap1*
94 cDNA containing exons 3-5 flanked by loxP sites upstream of the R554Q mutation in
95 endogenous exon 4 of the *Keap1* gene **(Fig. 1a)**[30]. For the Lox-STOP-Lox *(LSL)-*
96 *Nfe2l2^{D29H}* allele, we inserted a loxP-flanked transcriptional and translational STOP
97 (LSL) cassette upstream of the D29H mutation in exon 2 of the endogenous *Nfe2l2*
98 gene **(Fig. 1b).** For both alleles, Cre-mediated excision of loxP-flanked cassettes allows
99 for physiological expression of Keap1^{R554Q} or Nrf2^{D29H}, recapitulating NRF2 activation in

100 human NSCLC. To validate the functionality of these alleles, we first generated mouse
101 embryonic fibroblasts (MEFs), which allowed the switching from a Nrf2 deficient state
102 ($Nrf2^{LSL/LSL}$) to a Nrf2 stabilized state ($Nrf2^{D29H/D29H}$), or from a basal Nrf2 state
103 ($Keap1^{+/+}$) to a stabilized Nrf2 state ($Keap1^{R554Q/R554Q}$) in an isogenic system. Using
104 these MEFs, we performed both transcriptomic profiling **(Fig. 1c, d)**. RNA-sequencing
105 indicated that both $Keap1^{R554Q/R554Q}$ and $Nrf2^{D29H/D29H}$ MEFs demonstrated increased
106 transcription of canonical Nrf2 target genes, including Nqo1, Srxn1, Txnrd1, and Gclc
107 **(Fig. 1c, d)**. Prior targeting of the murine *Keap1* locus to generate a *Keap1*^{flox} allele
108 resulted in the generation of a hypomorphic allele prior to Cre-mediated recombination,
109 leading to decreased Keap1 levels and increased Nrf2 transcriptional activity throughout
110 the whole animal[40]. Importantly, we found no differences in expression of Keap1, Nrf2,
111 or Nrf2 target proteins Nqo1 and Gclc between CA-$Keap1^{R554Q}$ and WT Keap1 MEFs,
112 indicating that the *CA-Keap1*^{R554Q} allele is not hypomorphic (**Fig. S1**). Collectively, these
113 results indicate that the mutant *Keap1*^{R554Q} and *Nfe2l2*^{D29H} alleles activate the Nrf2
114 transcriptional program.
115
116 **Keap1 or Nrf2 mutation is not sufficient to initiate lung tumorigenesis**
117 Given the importance of NRF2 in cytoprotection and redox homeostasis, there has been
118 a longstanding interest in activating NRF2 pharmacologically for chemoprevention[8-10].
119 The long-term safety of this approach, and whether the chronic activation of NRF2 can
120 transform healthy cells *in vivo*, remains unknown. Moreover, the whole body deletion of
121 Keap1 in mice results in postnatal lethality because of constitutive Nrf2 activation[41]. In
122 human lung tumors, *KEAP1* inactivation is frequently biallelic[13], whereas *NFE2L2*
123 mutations are frequently heterozygous[42]. Therefore, we induced the recombination of
124 *Keap1* and *Nfe2l2* alleles in the lungs of $Keap1^{R554Q/+}$, $Keap1^{R554Q/R554Q}$, or $Nrf2^{D29H/+}$
125 mice using adenoviral-Cre to test whether constitutive Nrf2 activation is sufficient to
126 initiate lung tumor formation **(Fig. 2)**. First, we analyzed the overall survival between the
127 different groups. The median survival across genotypes ranged from approximately
128 650-750 days, with no significant survival differences observed between wild-type and
129 Keap1/Nrf2 mutant groups **(Fig. 2a)**. While mice did develop tumors, they comprised
130 age-associated tumors like lymphoma. Upon examination of mouse lung histology for

131 the presence of lung tumors, lung tumor-free survival was also not different between the
132 groups **(Fig. 2b)**. Finally, histological analysis of lung tissues revealed that both alveolar
133 and bronchiolar cells appeared phenotypically normal across the genotypes **(Fig. 2c)**.
134 These results indicate that constitutive Nrf2 activation is not sufficient to induce lung
135 tumor formation.
136
137 **Keap1 or Nrf2 mutation is not sufficient to initiate lung tumorigenesis in**
138 **combination with tumor suppressor loss**
139 To determine whether tumor suppressor loss was required for mutant Keap1 or Nrf2 to
140 initiate lung tumor formation, we crossed Keap1 and Nrf2 mutant mice with $p53^{flox}$ and
141 $Lkb1^{flox}$ alleles to concomitantly activate Nrf2 and delete these tumor suppressors in the
142 lung **(Fig. 3)**. We first examined the consequence of $Nrf2^{D29H/+}$, $Keap1^{R554Q/+}$, or
143 $Keap1^{R554Q/R554Q}$ in combination with p53 deletion. Mice were aged to 500 days, at
144 which time all mice were euthanized and examined for evidence of lung tumor
145 formation. While a small number of these mice did succumb to disease prior to 500
146 days, they developed age-associated tumors including lymphoma, and we did not
147 observe any differences in overall or lung tumor-free survival between genotypes **(Fig.**
148 **3a,b)**. However, when examining the lung tissue histology, we observed dysplasia in
149 $Keap1^{R554Q/R554Q}$ bronchioles following loss of p53 **(Fig. 3c)**. This observation is
150 consistent with previous work showing that tracheospheres derived from *Keap1*$^{-/-}$;*Trp53*$^{-}$
151 $^{/-}$ cells had an aberrant morphology[29]. We next examined the consequence of $Nrf2^{D29H/+}$,
152 $Keap1^{R554Q/+}$ or $Keap1^{R554Q/R554Q}$ in combination with Lkb1 deletion. Similar to what was
153 observed with p53, we also did not find any differences in overall or lung tumor-free
154 survival between cohorts **(Fig. 3d,e)**. Moreover, the bronchiolar and alveolar
155 morphology was normal across genotypes, in contrast to what was observed upon p53
156 loss **(Fig. 3f)**. Our findings indicate that Keap1/Nrf2 mutation is not sufficient to initiate
157 lung tumor formation in combination with tumor suppressor loss.
158
159 **Nrf2 activation cooperates with mutant Kras to promote lung tumor initiation and**
160 **early progression**

161 We and others have reported that Nrf2 activation is important for Kras mutant lung
162 tumorigenesis[21,27,28]. To understand how Keap1 or Nrf2 mutation affect lung tumor
163 initiation and early progression, we crossed Keap1/Nrf2 mutant mice with the Kras$^{G12D/+}$
164 model of early lung adenocarcinoma[43]. While all mice succumbed to lung tumors with a
165 median survival of around 200 days, we observed no difference in survival between
166 cohorts **(Fig. 4a,b)**. We next validated that these mutations were activating toward Nrf2
167 in tumors by performing immunohistochemical staining for Nrf2 and the Nrf2 target
168 Nqo1. We observed that Keap1$^{R554Q/R554Q}$ expression resulted in the greatest degree of
169 Nrf2 activation, followed by Nrf2$^{D29H/+}$, and then Keap1$^{R554Q/+}$ compared to Keap1/Nrf2$^{+/+}$
170 expression **(Fig. 4c-f)**. To examine the influence of Nrf2 activation on tumor initiation,
171 we quantified tumor number across the genotypes and found that Keap1$^{R554Q/R554Q}$ and
172 Nrf2$^{D29H/+}$ significantly increased tumor number in the Kras$^{G12D/+}$ model **(Fig. 4g,h)**,
173 consistent with prior reports using Keap1 deletion models[27,28]. We then examined the
174 influence of Nrf2 on tumor progression by analyzing tumor grade. The distribution of
175 atypical adenomatous and bronchiolar hyperplasia (AAH and BH, respectively) and
176 tumors from grades 1 (adenoma) to 5 (adenocarcinoma) was determined. We observed
177 an increased proportion of grade 1 tumors in Keap1$^{R554Q/R554Q}$ and Nrf2$^{D29H/+}$ mice
178 compared to Keap1$^{R554Q/+}$ and Keap1/Nrf2$^{+/+}$ mice **(Fig. 4i)**. Surprisingly, we found that
179 there was a decrease in grade 3 tumor burden across all Keap1 and Nrf2 mutant
180 models **(Fig. 4j)**, although these tumors were rare. Our findings indicate that Kras$^{G12D/+}$
181 mutation cooperates with Keap1/Nrf2 mutation to promote formation of lung tumors and
182 early progression to low-grade tumors.
183
184 **Nrf2 activation impairs lung adenocarcinoma progression**
185 The decrease in grade 3 tumor burden in the Keap1/Nrf2 mutant models suggested that
186 Nrf2 activation may impair progression to higher grade tumors. We next used the
187 Kras$^{G12D/+}$; p53$^{fl/fl}$ (KP) model, which develops advanced-grade lung adenocarcinomas[44].
188 We previously reported that the expression of Keap1$^{R554Q/R554Q}$ dramatically decreased
189 overall tumor size in this model[30], but other groups have found differing effects of Nrf2
190 activation. While some studies reported that Keap1 inactivation promoted
191 adenocarcinoma progression[31,32], others reported that Keap1 deletion did not affect

192 tumor size[34,35], but the conditions used and phenotypes assayed varied across these
193 studies. Thus, we decided to perform comprehensive phenotyping on KP tumors
194 following Nrf2 activation. Similar to what we observed in the $Kras^{G12D/+}$ model, we found
195 that overall survival of the KP model was not affected by Keap1 or Nrf2 mutation **(Fig.**
196 **5a,b)**. Moreover, we found that Keap1/Nrf2 mutation affected Nrf2 activation in a similar
197 manner to the $Kras^{G12D/+}$ model, with $Keap1^{R554Q/R554Q}$ being the most activating,
198 followed by $Nrf2^{D29H/+}$, and then $Keap1^{R554Q/+}$ compared to $Keap1/Nrf2^{+/+}$ mice **(Fig. 5c-**
199 **f)**. Next, we examined tumor progression by tumor grading and found a significant
200 decrease in the proportion of grade 3 and 4 tumors in the $Keap1^{R554Q/R554Q}$ cohort **(Fig.**
201 **5g,h)**. We also observed an increase in the proportion of grade 1 tumors with
202 $Keap1^{R554Q/R554Q}$, suggesting that there may be a threshold for Nrf2 activation to
203 promote early progression, but impair late progression **(Fig. 5h)**. Moreover, we found
204 similar trends by analyzing tumor burden by grade, as seen with an increase in grade 1
205 tumor burden and a decrease in grade 3 tumor burden with $Keap1^{R554Q/R554Q}$ **(Fig. 5i)**.
206 Although not statistically significant, the $Nrf2^{D29H/+}$ cohort also had a modest decrease in
207 grade 3 and 4 tumors, further supporting a threshold for Nrf2 to impair tumor
208 progression **(Fig. 5g-i)**. We next investigated whether tumors that progressed to the
209 adenocarcinoma stage altered Nrf2 expression and/or activity. To this end, we analyzed
210 Nrf2 and Nqo1 levels across all tumor grades and hyperplasia (AAH, BH). We found
211 that Nrf2 and Nqo1 levels were highly elevated in Keap1/Nrf2 mutant grade 1 tumors,
212 with Nqo1 demonstrating increased nuclear localization in homozygous Keap1 mutant
213 tumors compared to Nrf2 mutant tumors **(Fig. 6a)**. However, as tumors progressed to
214 higher grades, Nrf2 and Nqo1 expression were reduced in the Keap1/Nrf2 mutant
215 models **(Fig. 6a-c)**. These results suggest that Nrf2 activation beyond a certain
216 threshold impairs advanced-grade tumor progression, requiring selection for a more
217 tolerable level of Nrf2 expression and activity in high-grade tumors.
218

219 **NRF2 overexpression impairs NSCLC cell proliferation, viability, and anchorage-**
220 **independent colony formation**

221 KEAP1 has other substrates[45-50], raising the question of whether NRF2 plays a causal
222 role in tumor suppression. It was previously reported that KEAP1 mutant lung cancer

223 cell lines are “NRF2 addicted” and dependent on NRF2 for proliferation[51]. Supportingly,
224 analysis of DepMap data[52] revealed that NSCLC cell lines with high NRF2 activity[22],
225 which were enriched for KEAP1 mutations, exhibited NRF2 dependence **(Fig. 7a)**. To
226 directly test the hypothesis that excessive NRF2 activation above a specific threshold is
227 detrimental to lung tumor cell growth, we used lentiviral transduction to overexpress
228 NRF2 in five KEAP1 mutant lung cancer cell lines (H1944, H322, A549, HCC15, H460).
229 We confirmed overexpression of NRF2 by western blot analysis of NRF2 and target
230 genes GCLC, xCT, and GSR **(Fig. 7b)**. Lentiviral transduction increased the expression
231 of NRF2 in all cell lines, and also increased the expression of NRF2 targets,
232 demonstrating that NRF2 binding sites were not saturated by the level of NRF2 in these
233 cell lines **(Fig. 7b)**. Next, we determined the influence of NRF2 overexpression on
234 cellular proliferation and death over the course of four days using live cell imaging **(Fig.
235 7c-g)**. We found that NRF2 overexpression decreased cell proliferation in all cell lines,
236 and increased cell death in 4 out of 5 cell lines **(Fig. 7f,g)**. Finally, we observed
237 impaired anchorage-independent growth in soft agar in all cell lines **(Fig. 7h,i)**. These
238 results indicate that there is an optimal threshold of NRF2 activity, and that excess
239 NRF2 activation can impair lung cancer phenotypes.
240
241 **Single copy Nrf2 deletion rescues homozygous Keap1^{R554Q}-mediated tumor
242 progression impairment**
243 To directly examine whether reducing Nrf2 levels could alleviate the block in
244 adenocarcinoma progression in the Keap1$^{R554Q/R554Q}$ model, we crossed a Nrf2^{flox} allele
245 into both our Kras$^{G12D/+}$; p53$^{fl/fl}$ and Kras$^{G12D/+}$; p53$^{fl/fl}$; Keap1$^{R554Q/R554Q}$ models. Because
246 we previously found that complete Nrf2 deficiency impairs tumor initiation[21], we
247 examined the consequence of single copy Nrf2 deletion on tumor phenotypes. Again,
248 we found no difference in overall survival between groups **(Fig. 8a)**. We also observed
249 that Nrf2 deletion in the Keap1$^{R554Q/R554Q}$ model significantly decreased expression of
250 Nrf2 and Nqo1 **(Fig. 8b-e, S2)**. Moreover, histological examination of the lungs revealed
251 a striking difference in tumor number and size, with Nrf2 heterozygous deletion having a
252 minimal effect on the Kras$^{G12D/+}$; p53$^{fl/fl}$ model while dramatically increasing tumor
253 burden in the Kras$^{G12D/+}$; p53$^{fl/fl}$; Keap1$^{R554Q/R554Q}$ model **(Fig. 8f).** Next, we examined

254 tumor progression in these models. In agreement with our previous experiment **(Fig.**
255 **5h)**, we found that the Keap1$^{R554Q/R554Q}$ cohort had a significant reduction in
256 adenocarcinoma progression upon Nrf2^{WT} expression **(Fig. 8g)**. However, upon single
257 copy Nrf2 deletion (Nrf2$^{flox/+}$), Keap1$^{R554Q/R554Q}$ failed to suppress tumor progression
258 **(Fig. 8g)**. Similar findings were observed when analyzing tumor burden by grade, with a
259 decrease in grade 3 tumor burden induced by Keap1$^{R554Q/R554Q}$ that was alleviated by
260 single copy deletion of Nrf2 **(Fig. 8h)**. These results demonstrate that there is a
261 threshold by which Nrf2 activation can promote or impair tumor initiation or progression.
262

263 **Discussion**
264

265 Using genetically engineered mouse models of Keap1/Nrf2 mutation, we find that
266 Keap1 or Nrf2 mutations alone are insufficient to cause lung tumor formation. Even in
267 combination with tumor suppressor loss, we did not observe lung tumor formation after
268 500 days, suggesting that chronic NRF2 activation would be a safe strategy for
269 chemoprevention. These findings corroborate previous studies showing that Keap1
270 deletion does not induce lung tumor development[26], even in the absence of tumor
271 suppressors p53 or Lkb1[27], out to 12-15 months. In combination with Kras$^{G12D/+}$
272 mutation, we found that Nrf2 activation promoted tumor initiation. Our results are
273 consistent with previous work indicating that Nrf2 activation via Keap1 deletion
274 promotes Kras$^{G12D/+}$ tumor initiation[27,28]. Surprisingly, we find that Nrf2 activation impairs
275 tumor progression, which is correlated with Nrf2 dosage. In our previous study with
276 Keap1$^{R554Q/R554Q}$ mice, we reported smaller tumors in the KP model[30], which we now
277 find is due to impaired tumor progression mediated by Nrf2 hyperactivation. Because
278 most prior studies from other groups did not specifically analyze tumor grade[25,27,34,35],
279 they may not have captured this effect of Nrf2 on tumor progression. Alternatively, there
280 may be biological differences between Keap1 deletion and mutation.
281

282 Our findings that tumors downregulate Nrf2 to select for a level permissive for tumor
283 progression and that ectopic NRF2 expression antagonizes the proliferation and viability
284 of human NSCLC cells are supported by our finding that single copy deletion of Nrf2
285 can rescue the homozygous Keap1^{R554Q}-mediated block in tumor progression. This

286 result demonstrates a direct role for Nrf2 hyperactivation but we cannot exclude the
287 possibility that alternative KEAP1 substrates, such as PGAM5[45], PALB2[46], MCM3[47] or
288 EMSY[48], contribute to the block in tumor progression. In agreement with our findings, a
289 Keap1-binding defective Nrf2^{E79Q} mouse model of small-cell lung cancer (SCLC) with
290 p53/ p16 inactivation[53] also displayed Nrf2 downregulation in aggressive SCLC tumors.
291 The exact mechanism(s) by which high NRF2 activity impairs tumor cell proliferation
292 and tumor progression remains to be determined. The dosage-dependent effects of
293 Nrf2 are reminiscent of what has been observed for oncogenes like Ras and Myc,
294 where low levels promote transformation and proliferation, and high levels promote
295 senescence or death[54,55].
296
297 Given that KEAP1 and NRF2 mutations are found with a high frequency in human
298 NSCLC and are associated with poor outcomes, these findings raise the question of
299 under which contexts NRF2 activation provides an advantage. Our findings that
300 NRF2/KEAP1 mutation promotes tumor initiation are consistent with recent results from
301 the TRACERx study, where *KEAP1* mutations were found to be an initiating driver
302 together with *KRAS* and *TP53* mutations in lung adenocarcinoma[56], and suggest that
303 additional genetic events may be needed to overcome NRF2-mediated inhibition of
304 tumor progression. We did not find that these mutations conferred poor outcomes in our
305 mouse models, but there are multiple features of patient tumors not captured by our
306 models that remain to be examined. They did not develop metastases with sufficient
307 frequency, precluding an examination of the influence of Nrf2 activation on metastasis
308 as reported previously[25]. Moreover, mice are not exposed to smoking and other
309 environmental toxins under which NRF2 activation may promote survival[4-7]. We have
310 also not tested the response of these models to therapy. Overall, our work
311 demonstrates the context-dependence of the role of NRF2 during the complex stages of
312 tumorigenesis and warrants further investigation into how NRF2 elicits distinct
313 responses.
314
315 **Methods**
316

317 **Mice**

318 Mice were housed and bred in accordance with the ethical regulations and approval of
319 the IACUC (protocols #: IS00003893R and IS00007922R). Generation of the Keap1
320 targeting vector was previously described[30]. Briefly, the *CA-Keap1*^{R554Q} allele
321 (Keap1^{tm1Gmdn}, MGI: 7327097) was made by inserting a wild-type *Keap1* cDNA
322 containing exons 3-5 flanked by loxP sites upstream of the R554Q mutation in exon 4 of
323 the *Keap1* gene. *Keap1* was targeted in C10 murine ES cells and cells were selected
324 with blasticidin. To make the *LSL-Nfe2l2*^{D29H} allele (Nfe2l2^{tm1Gmdn}, MGI: 7327101), a
325 STOP cassette flanked by loxP sites was inserted into intron 1 and codon 29 in
326 endogenous exon 2 was mutated from an aspartic acid to a histidine. The endogenous
327 *Nfe2l2* locus was targeted in C10 murine ES cells and puromycin was used to select
328 positive cells. For both alleles, positive clones were screened by copy number real-time
329 PCR and injected into blastocysts. Genotyping primers were as follows: for the
330 *Keap1*^{R554Q} allele: Mutant forward: 5'-ATGGCCACACTTTTCTGGAC-3'; wild-type (WT)
331 forward: 5'-GGGGGTAGAGGGAGGAGAAT-3'; Common reverse: 5'-
332 GCCACCCTATTCACAGACCA-3'. The WT PCR product was 326 bp and the mutant
333 PCR product 584 bp. For the *Nfe2l2*^{D29H} allele: WT forward: 5'-
334 GAGGCAGGTAGTTCTCTGAGTTTG-3'; Common reverse: 5'-
335 GCAAATGCACTGAGACACTCAT-3'; Mutant forward: 5'-
336 CTAGCCACCATGGCTTGAGT-3'. The WT PCR product was 189 bp and the mutant
337 PCR product 282 bp. All mice were maintained on a mixed C57BL/6 genetic
338 background. In addition to Keap1^{R554Q} and Nrf2^{D29H} mice, p53^{flox}
339 (RRID:IMSR_JAX:008462); Lkb1^{flox} (RRID:IMSR_JAX:014143); Nrf2^{flox}
340 (RRID:IMSR_JAX:025433); and LSL-Kras$^{G12D/+}$ (RRID:IMSR_JAX:008179) mice were
341 used. For mouse lung tumor studies, intranasal installation of 2.5 x 10^7 PFU adenoviral-
342 Cre (University of Iowa) was used to induce lung tumors as previously described[43].
343 Adenoviral infections were performed under isofluorane anesthesia.
344

345 **Murine embryonic fibroblast generation and culture**

346 MEFs were isolated from E13.5-14.5-day old embryos and maintained in pyruvate-free
347 DMEM (Corning) containing 10% FBS, 100 units/mL penicillin and 100 µg/mL

348 streptomycin (Gibco) in a humidified incubator with 5% CO_2 and 95% air at 37°C. MEFs
349 were used within four passages and infected with control empty adenovirus or
350 adenoviral-Cre (University of Iowa) at an approximate multiplicity of infection of 500.
351
352 **RNA-sequencing preparation and analysis**
353 Samples were prepared using the RNeasy plus mini kit (Qiagen, 74134). RNA quality
354 was checked with the QIAxcel RNA QC kit (Qiagen, 929104). Additional RNA QC,
355 sequencing, mapping to the mouse genome, and analysis were performed by
356 Novogene. Differentially expressed genes (DESeq2) with $p < 0.05$ were included in the
357 volcano plot.
358
359 **Immunohistochemistry (IHC)**
360 Mouse lung tissue was fixed with 10% formalin overnight, transferred to 70% ethanol
361 and paraffin embedded to be sectioned. Unstained tissue sections were de-paraffinized
362 in xylene followed by rehydration in a graded alcohol series. Antigen retrieval was
363 performed by boiling in 10mM citrate buffer (pH 6). Antibodies used for IHC include
364 affinity-purified NRF2 (1:150 or 1:300)[57] and NQO1 (Sigma Aldrich, RRID:AB_1079501,
365 1:500). Following overnight incubation at 4°C in primary antibody, the ImmPRESS HRP
366 goat anti-rabbit kit (Vector Laboratories, RRID:AB_2631198) was used as directed by
367 manufacturer's instructions. DAB peroxidase (HRP) substrate (Vector Laboratories, SK-
368 4105) was used to develop immunohistochemical staining, followed by counterstaining
369 with hematoxylin (Vector Laboratories, H-3404). Slides were scanned with the Aperio
370 imager at 20x and the H-score of at least five representative regions/ mouse was
371 analyzed with QuPath software[58]. Representative images were captured using the Axio
372 Lab.A1 microscope at 40x (Carl Zeiss Microimaging Inc.).
373
374 **Tumor grading analysis and histology**
375 Lung tumor grading was performed manually as previously described[44]. Tumor grading
376 distribution percentages were calculated by dividing the number of tumors in a specific
377 grade by the total number of tumors per mouse. Tumor burden by grade was calculated
378 by dividing the area of the lung covered by a specific tumor grade by the total lung area.

379

380 **NSCLC cell lines and culture**

381 Human lung cancer cell lines used include H1944 (RRID:CVCL_1508), H322
382 (RRID:CVCL_1556), A549 (RRID:CVCL_0023), HCC15 (RRID:CVCL_2057), and H460
383 (RRID:CVCL_0459) and were previously described[22]. Cells were cultured in RPMI 1640
384 (Gibco) containing 5% FBS without antibiotics in a humidified incubator with 5% CO_2
385 and 95% air at 37°C. Cells were screened regularly and confirmed to be free of
386 mycoplasma with the MycoAlert kit (Lonza).

387

388 **Lentivirus generation and infection of NSCLC cells**

389 Lentiviruses were made by transfecting Lenti-X 293T cells (Takara 632180) overnight
390 with polyethylenimine (PEI), lentiviral plasmid (pLX317-NRF2[59] or the control pLX317
391 empty vector[30]), and packaging plasmids pCMV-dR8.2 dvpr (RRID:Addgene_8455) and
392 pCMV-VSV-G (RRID:Addgene_8454) in DMEM containing 10% FBS. To generate
393 NRF2-overexpressing cells, NSCLC cells were transduced for 24 hrs with lentiviruses in
394 medium containing polybrene (8 µg/mL). After transduction, infected cells were selected
395 with 0.5 µg/mL (H1944, H322, H460) or 1 µg/mL (A549, HCC15) puromycin for 72 hrs.
396 Immediately following selection, cells were seeded in respective puromycin
397 concentrations for the indicated assays.

398

399 **Cell proliferation and cell death assays**

400 NSCLC cells were monitored with the CELLCYTE X™ live cell imaging instrument
401 (Cytena) over the course of 96 hours. Prior to imaging, SYTOX Green nucleic acid stain
402 (Thermo Fisher Scientific, S7020) was added to medium at a final concentration of 20
403 nM. Images were acquired from each well at 8-hour intervals and analyzed using
404 CellCyte Studio (CELLINK). Cell confluency was represented as the % of the image
405 covered by cells. The number of dead cells was normalized to cell confluency [number
406 of Sytox Green positive cells/ mm^2/ cell confluency]. The area under the curve (AUC)
407 values were calculated by summing the proliferation or normalized dead cell number at
408 each time point.

409

410 **Western blotting**

411 Cells were lysed in ice-cold RIPA buffer with protease inhibitors (Fisher Scientific,
412 PIA32955) followed by sonication in a water bath sonicator (Diagenode). Protein was
413 quantified using the DC protein assay (Bio-Rad). Lysates were prepared with 6X SDS
414 sample buffer containing 12% (v/v) β-ME (VWR) and separated on Bolt™ or NuPAGE
415 4-12% Bis-Tris gels (Invitrogen). SDS-PAGE separation was followed by transfer to
416 0.45 µm nitrocellulose membranes (GE Healthcare). The membranes were blocked in
417 5% non-fat milk in Tris-buffered saline with 0.1% Tween 20 (TBST). For immunoblotting,
418 the following antibodies diluted in 5% milk in TBST were used: KEAP1 (Millipore Sigma,
419 RRID:AB_2921362, 1:2000), NRF2 (Cell Signaling Technologies, D1Z9C,
420 RRID:AB_2715528, 1:1000), NQO1 (Sigma Aldrich, RRID:AB_1079501, 1:1000), GCLC
421 (Sana Cruz Biotechnology, H-5, RRID:AB_2736837, 1:1000), xCT (abcam,
422 RRID:AB_778944, 1:1000), GSR (Santa Cruz Biotechnology, RRID:AB_2295121,
423 1:1000), β-actin (Invitrogen AM4302, RRID:AB_2536382, 1:100,000). HRP secondary
424 antibodies used include goat anti-rabbit IgG (Jackson ImmunoResearch Labs, RRID:
425 AB_23135627), goat anti-mouse IgG (Jackson ImmunoResearch Labs,
426 RRID:AB_10015289), and goat anti-rat IgG (Jackson ImmunoResearch Labs,
427 RRID:AB_2338128). Membranes were developed with Clarity ECL substrate (Bio-Rad)
428 or a luminol-based homemade ECL substrate.

429

430 **Soft agar colony formation assays**

431 6-well plates were coated with a 0.8% agar prepared in RPMI. NSCLC cells were then
432 seeded in 0.4% agar in RPMI. After the cell/ agar mixture solidified, RPMI medium
433 containing 10% FBS, Pen/Strep and puromycin was added to each well and replenished
434 every few days. Colonies were allowed to form for 10–16 days, and wells were stained
435 with 0.01% crystal violet in a 4% paraformaldehyde in PBS solution. Plates were
436 scanned on a flatbed scanner and ImageJ was used to quantify colonies.

437

438 **DepMap Analysis**

439 *NFE2L2* dependency scores were downloaded from the DepMap database v. 22Q2[52].
440 Values were plotted from CRISPR (DepMap 22Q2 Public+Score, Chronos) for non-

441 small cell lung cancer cell lines that we previously evaluated for high or low NRF2
442 activity[22].
443
444 **Statistical analysis**
445 Graphpad Prism9 software was used for statistical analyses and P values < 0.05 were
446 considered significant, with symbols as follows: *p<0.05, **p<0.01, ***p<0.001,
447 ****p<0.0001. All data is represented as mean +/- standard deviation unless otherwise
448 stated. For all experiments, similar variances between groups were observed.
449
450 **Online supplemental material**
451 **Fig. S1** shows that the *CA-Keap1*^{R554Q} allele does not exhibit hypomorphism in mouse
452 embryonic fibroblasts. **Fig. S2** shows the H-scores by tumor grade of Nrf2 and Nqo1
453 immunohistochemical staining in Kras$^{G12D/+}$; p53$^{fl/fl}$ and Kras$^{G12D/+}$; p53$^{fl/fl}$;
454 Keap1$^{R554Q/R554Q}$ mouse models with single copy Nrf2 deletion.
455
456 **Acknowledgements**
457 This work was supported by grants from the NIH/NCI (R37-CA230042), the American
458 Lung Association (LCDA-498544) and the American Cancer Society's Institutional
459 Research Grant to G.M.D. This work was also supported by the Analytical Microscopy
460 and the Tissue Core Facilities at the Moffitt Cancer Center, an NCI designated
461 Comprehensive Cancer Center (P30-CA076292). We would like to thank the DeNicola
462 lab members and Dr. Ana Gomes for the helpful discussions. We thank Cheyenne
463 Schneider for proofreading.
464
465 **Author Contributions**
466 G.M.D. conceived the project and G.M.D. and J.M.D. designed the experiments.
467 G.M.D., I.I.C.C. and F.A.K. designed and generated the Nrf2 and Keap1 mutant mice.
468 G.M.D. performed the RNA sequencing. Maintenance of animal colonies, generation of
469 experimental animals, and collections of tissues were performed by A.F., with
470 assistance from S.C. and N.F.P. J.M.D. performed cell line experiments,
471 immunohistochemistry, and tumor histology analyses. J.R.P. and E.E.S. generated the

472 affinity-purified NRF2 antibody used for immunohistochemistry. J.M.D. and G.M.D.
473 wrote the manuscript, and all authors reviewed it. G.M.D. acquired funding and
474 supervised the study.
475
476 **Competing interests**
477 The authors declare no competing financial or personal interests.
478
479 **Additional information**
480 Correspondence and requests for materials should be addressed to G.M.D.

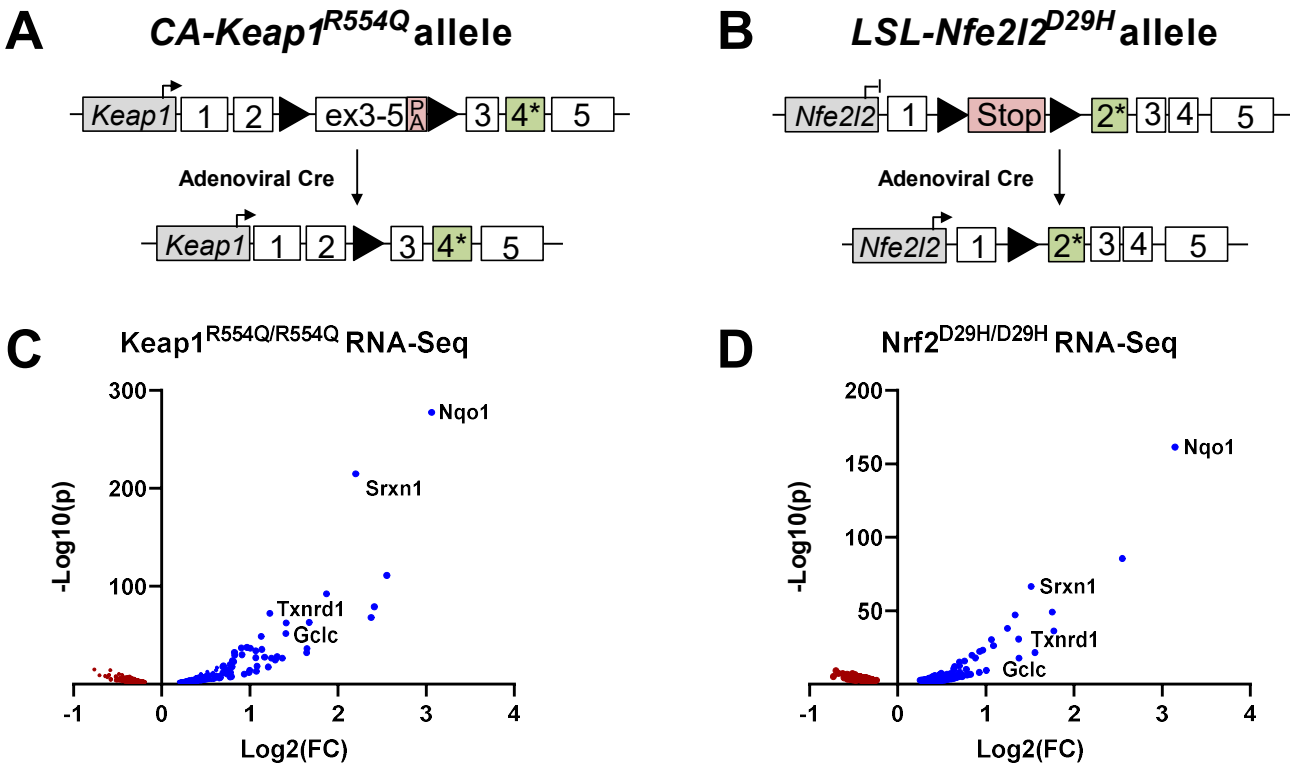
A
CA-Keap1R554Q allele
Keap1
1
2
ex3-5
PA
3
4*
5
Adenoviral Cre
B
LSL-Nfe2l2D29H allele
Nfe2l2
Stop
C
Keap1R554Q/R554Q RNA-Seq
-Log10(p)
Log2(FC)
Nqo1
Srxn1
Txnrd1
Gclc
D
Nrf2D29H/D29H RNA-Seq

481 **Figure 1. Development of mutant *Keap1* and *Nfe2l2* alleles found in human lung**
482 **cancer. (A)** The conditionally active (CA)-*Keap1*^{R554Q} allele was generated by inserting
483 a loxP-flanked, wild type (WT) *Keap1* cDNA containing exons 3-5 into intron 2 and
484 introducing the R554Q mutation into endogenous exon 4 of the *Keap1* gene. Prior to
485 intranasal installation of adenoviral-Cre recombinase Keap1 is wild type. Once the
486 floxed cargo is excised, mutant Keap1^{R554Q} is expressed. PA = poly A signal. **(B)** The
487 Lox-STOP-Lox *(LSL)-Nfe2l2*^{D29H} allele was created by inserting a STOP cassette
488 flanked by loxP sites into intron 1 and introducing the D29H mutation in endogenous
489 exon 2 of the *Nfe2l2* gene. Following Cre-mediated excision of the STOP cassette,
490 mutant Nrf2^{D29H} is expressed. **(C)** Volcano plot of RNA-sequencing data from murine
491 embryonic fibroblasts (MEFs) expressing Keap1$^{R554Q/R554Q}$ compared to Keap1$^{+/+}$. N=3,
492 representative of two individual MEF lines. **(D)** Volcano plot of RNA-sequencing data
493 from MEFs expressing Nrf2$^{D29H/D29H}$ compared to Nrf2$^{LSL/LSL}$, which lack Nrf2 expression.
494 N=3, representative of two individual MEF lines.

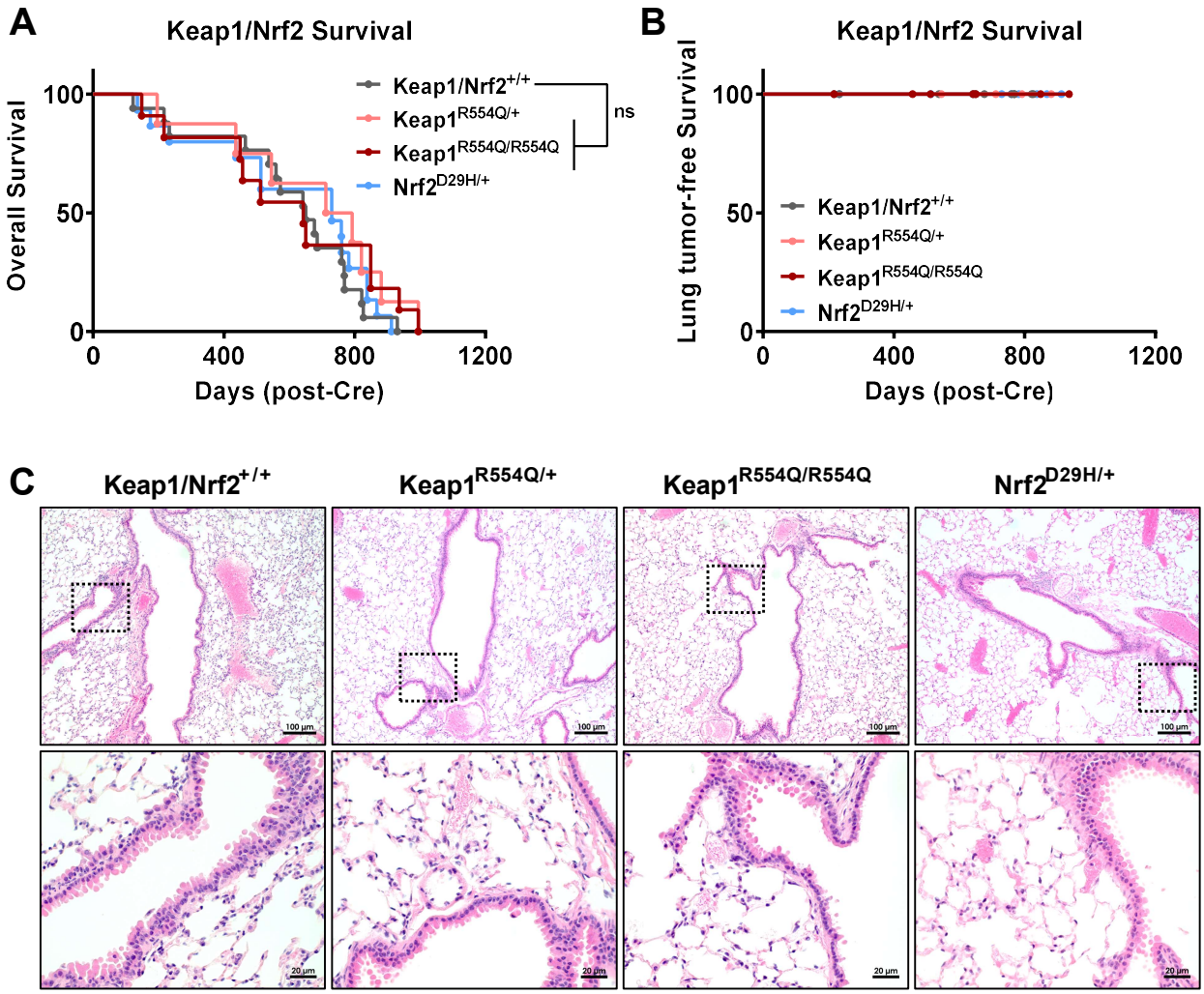
A
Keap1/Nrf2 Survival
Overall Survival
100
50
0
0
400
800
1200
Days (post-Cre)
Keap1/Nrf2+/+
Keap1R554Q/+
Keap1R554Q/R554Q
Nrf2D29H/+
ns
B
Keap1/Nrf2 Survival
Lung tumor-free Survival
100
50
0
0
400
800
1200
Days (post-Cre)
Keap1/Nrf2+/+
Keap1R554Q/+
Keap1R554Q/R554Q
Nrf2D29H/+
C
Keap1/Nrf2+/+
Keap1R554Q/+
Keap1R554Q/R554Q
Nrf2D29H/+
100 µm
20 µm

495 **Figure 2. Mutation of Keap1 or Nrf2 is not sufficient to initiate lung tumorigenesis.**
496 **(A)** Overall survival of Keap1/Nrf2 mutant mice. Keap1/Nrf2$^{+/+}$ (n=17), Keap1$^{R554Q/+}$
497 (n=8); Keap1$^{R554Q/R554Q}$ (n=11); Nrf2$^{D29H/+}$ (n=15). Ns= not significant (Log-rank (Mantel-
498 Cox) test). **(B)** Lung tumor-free survival of Keap1/Nrf2 mutant mice. Keap1/Nrf2$^{+/+}$
499 (n=11), Keap1$^{R554Q/+}$ (n=4); Keap1$^{R554Q/R554Q}$ (n=8); Nrf2$^{D29H/+}$ (n=11). **(C)** Representative
500 H&E of mouse lung depicting normal bronchiolar and alveolar cells (scale bars = 100μM
501 (top panel), 20 μM (bottom panel)).

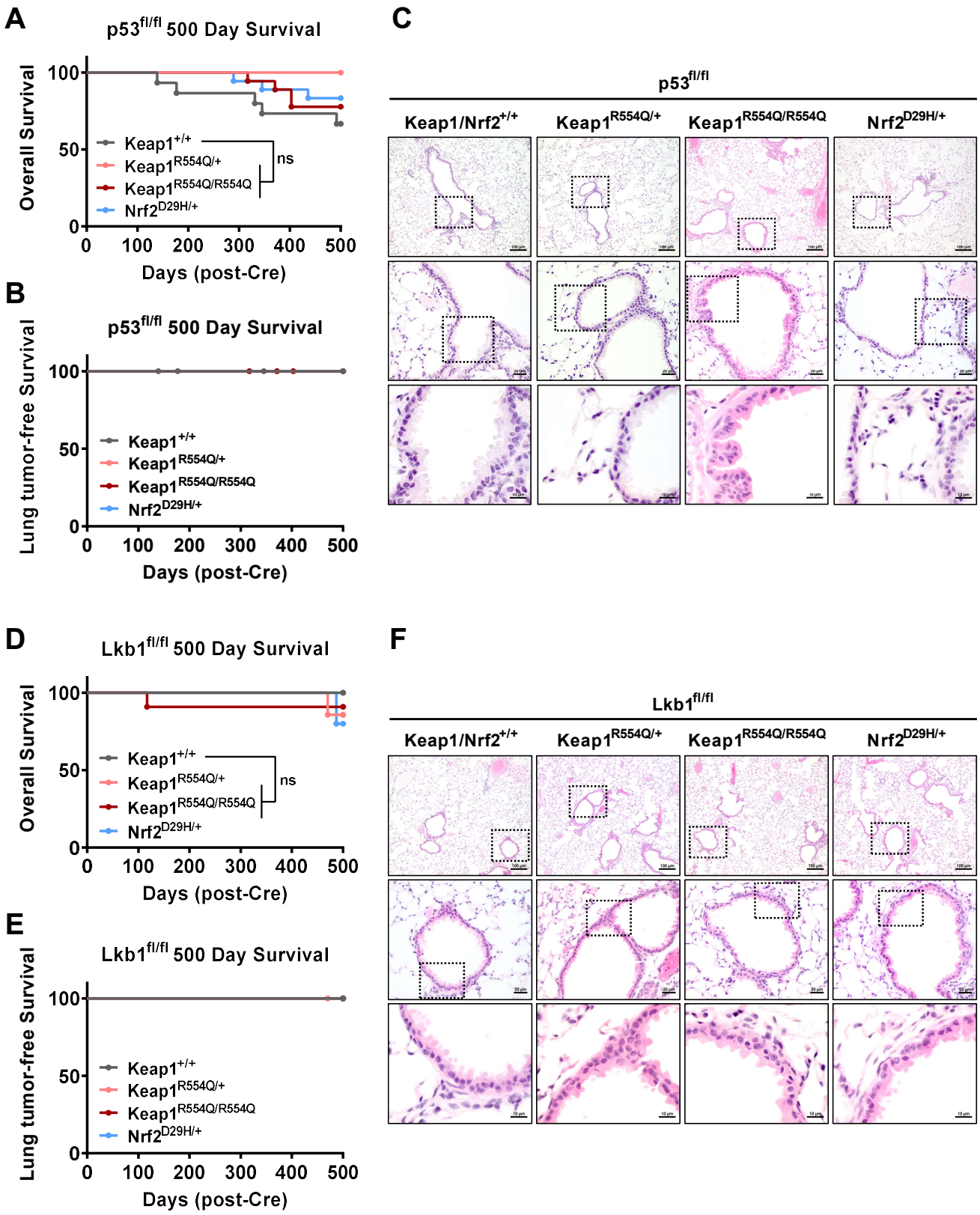
A
p53fl/fl 500 Day Survival
Overall Survival
100
50
0
Keap1+/+
Keap1R554Q/+
Keap1R554Q/R554Q
Nrf2D29H/+
ns
0 100 200 300 400 500
Days (post-Cre)
B
p53fl/fl 500 Day Survival
Lung tumor-free Survival
100
50
0
Keap1+/+
Keap1R554Q/+
Keap1R554Q/R554Q
Nrf2D29H/+
0 100 200 300 400 500
Days (post-Cre)
C
p53fl/fl
Keap1/Nrf2+/+
Keap1R554Q/+
Keap1R554Q/R554Q
Nrf2D29H/+
D
Lkb1fl/fl 500 Day Survival
Overall Survival
100
50
0
Keap1+/+
Keap1R554Q/+
Keap1R554Q/R554Q
Nrf2D29H/+
ns
0 100 200 300 400 500
Days (post-Cre)
E
Lkb1fl/fl 500 Day Survival
Lung tumor-free Survival
100
50
0
Keap1+/+
Keap1R554Q/+
Keap1R554Q/R554Q
Nrf2D29H/+
0 100 200 300 400 500
Days (post-Cre)
F
Lkb1fl/fl
Keap1/Nrf2+/+
Keap1R554Q/+
Keap1R554Q/R554Q
Nrf2D29H/+

502 **Figure 3. Mutation of Keap1 or Nrf2 is not sufficient to initiate lung tumorigenesis**
503 **with p53 or Lkb1 loss. (A)** Overall survival of $p53^{fl/fl}$ mice expressing wild-type or
504 mutant Keap1/Nrf2. $Keap1/Nrf2^{+/+}$ (n=15); $Keap1^{R554Q/+}$ (n=7); $Keap1^{R554Q/R554Q}$ (n=18);
505 $Nrf2^{D29H/+}$ (n=18). Ns= not significant (Log-rank (Mantel-Cox) test). **(B)** Lung tumor-free
506 survival of $p53^{fl/fl}$ mice expressing wild-type or mutant Keap1/Nrf2. $Keap1/Nrf2^{+/+}$ (n=11);
507 $Keap1^{R554Q/+}$ (n=6); $Keap1^{R554Q/R554Q}$ (n=16); $Nrf2^{D29H/+}$ (n=10). **(C)** Representative H&E
508 of mouse lung depicting bronchiolar and alveolar cells of the $p53^{fl/fl}$ models (scale bars =
509 100μM (top panel), 20μM (middle panel), 10μM (bottom panel)). **(D)** Overall survival of
510 $Lkb1^{fl/fl}$ mice expressing wild-type or mutant Keap1/Nrf2. $Keap1/Nrf2^{+/+}$ (n=11);
511 $Keap1^{R554Q/+}$ (n=7); $Keap1^{R554Q/R554Q}$ (n=11); $Nrf2^{D29H/+}$ (n=5). Ns= not significant (Log-
512 rank (Mantel-Cox) test). **(E)** Lung tumor-free survival of $Lkb1^{fl/fl}$ mice expressing wild-
513 type or mutant Keap1/Nrf2. $Keap1/Nrf2^{+/+}$ (n=11); $Keap1^{R554Q/+}$ (n=6); $Keap1^{R554Q/R554Q}$
514 (n=9); $Nrf2^{D29H/+}$ (n=4). **(F)** Representative H&E of mouse lung depicting bronchiolar and
515 alveolar cells of the $Lkb1^{fl/fl}$ models (scale bars = 100μM (top panel), 20μM (middle
516 panel), 10μM (bottom panel)). For **A, B, D, E,** mice were infected intranasally with
517 adenoviral-Cre, followed by collection at 500 days to analyze lung tissue histology.

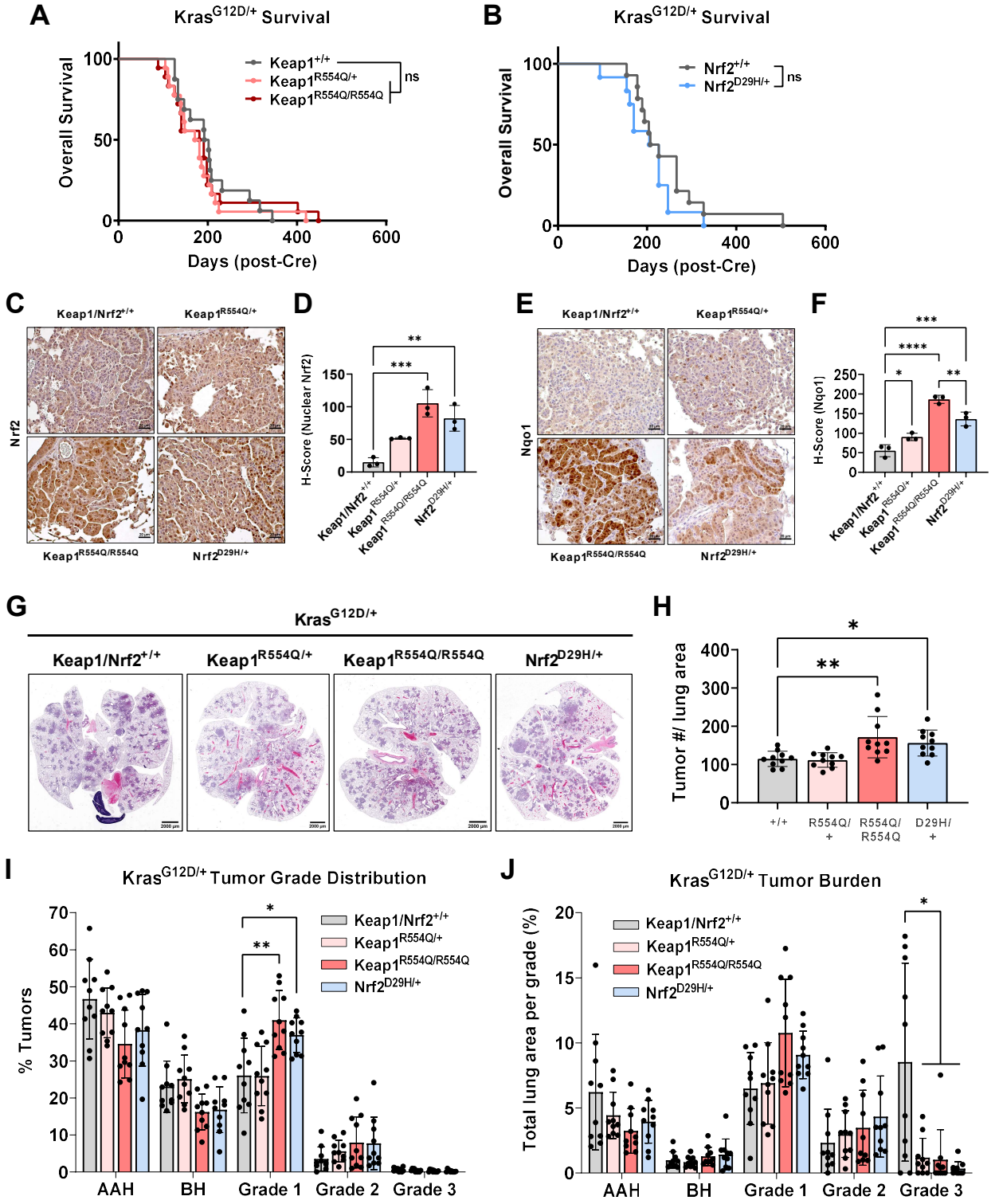
A
KrasG12D/+ Survival
Overall Survival
Days (post-Cre)
Keap1+/+
Keap1R554Q/+
Keap1R554Q/R554Q
ns
B
KrasG12D/+ Survival
Nrf2+/+
Nrf2D29H/+
C
Keap1/Nrf2+/+
Keap1R554Q/+
Nrf2
Keap1R554Q/R554Q
Nrf2D29H/+
D
H-Score (Nuclear Nrf2)
E
Nqo1
F
H-Score (Nqo1)
G
KrasG12D/+
H
Tumor #/ lung area
+/+
R554Q/+
R554Q/R554Q
D29H/+
I
KrasG12D/+ Tumor Grade Distribution
% Tumors
AAH
BH
Grade 1
Grade 2
Grade 3
J
KrasG12D/+ Tumor Burden
Total lung area per grade (%)

518 **Figure 4. Keap1/Nrf2 mutation cooperates with Kras$^{G12D/+}$ to promote lung tumor**
519 **initiation and early progression. (A)** Overall survival of Keap1 mutant mice with
520 Kras$^{G12D/+}$ mutation. Keap1$^{+/+}$ (n=16); Keap1$^{R554Q/+}$ (n=18); Keap1$^{R554Q/R554Q}$ (n=18). **(B)**
521 Overall survival of Nrf2 mutant mice with Kras$^{G12D/+}$ mutation. Nrf2$^{+/+}$ (n=14); Nrf2$^{D29H/+}$
522 (n=12). Ns = not significant (Log-rank (Mantel-Cox) test). **(C)** Representative
523 immunohistochemical (IHC) staining of Nrf2 in Keap1/Nrf2 mutant tumors with
524 Kras$^{G12D/+}$ mutation (scale bars = 20 μM). **(D)** H-scores for Nrf2 (nuclear) IHC staining.
525 **(E)** Representative immunohistochemical (IHC) staining of Nrf2 target Nqo1 (scale bars
526 = 20 μM). **(F)** H-scores for Nqo1 (whole cell) IHC staining. For **C-F**, N=3 mice per
527 genotype and >20,000 tumor cells per mouse. *p<0.05 (one-way ANOVA). **(G)**
528 Representative whole lung H&E-stained section (scale bars = 2000 μM). **(H)** Tumor
529 number per mouse in Keap1/Nrf2 mutant models normalized to lung area. *p<0.05 (one-
530 way ANOVA). **(I)** Distribution of tumor grades across Keap1/Nrf2 mutant models.
531 *p<0.05 (unpaired t test with Holm-Sidak's multiple comparisons test). AAH = atypical
532 adenomatous hyperplasia. BH = bronchiolar hyperplasia. **(J)** Fraction of lung tumor
533 burden by grade (lung tumor area/ total lung area per grade). *p<0.05 (unpaired t test
534 with Holm-Sidak's multiple comparisons test). For both **(I)** and **(J)** n=10 mice and ≥2,000
535 tumors per genotype.

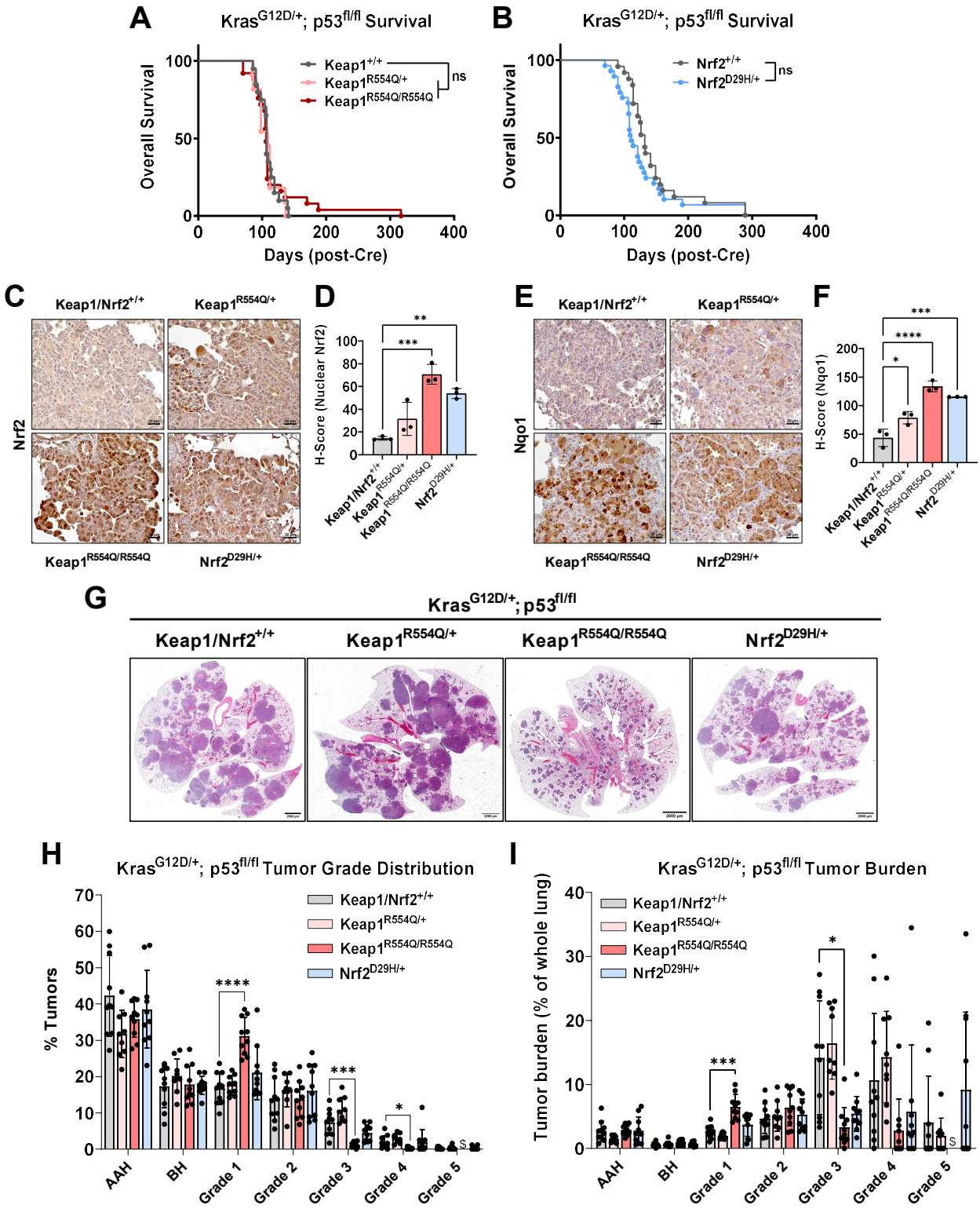
A
KrasG12D/+; p53fl/fl Survival
Overall Survival
Days (post-Cre)
Keap1+/+
Keap1R554Q/+
Keap1R554Q/R554Q
ns
B
KrasG12D/+; p53fl/fl Survival
Nrf2+/+
Nrf2D29H/+
C
Keap1/Nrf2+/+
Keap1R554Q/+
Nrf2
Keap1R554Q/R554Q
Nrf2D29H/+
D
H-Score (Nuclear Nrf2)
E
Nqo1
F
H-Score (Nqo1)
G
KrasG12D/+; p53fl/fl
H
KrasG12D/+; p53fl/fl Tumor Grade Distribution
% Tumors
AAH
BH
Grade 1
Grade 2
Grade 3
Grade 4
Grade 5
I
KrasG12D/+; p53fl/fl Tumor Burden
Tumor burden (% of whole lung)

536 **Figure 5. Homozygous Keap1^{R554Q} impairs adenocarcinoma progression in the**
537 **Kras$^{G12D/+}$; p53$^{fl/fl}$ model. (A)** Overall survival of Kras$^{G12D/+}$; p53$^{fl/fl}$ mice with Keap1
538 mutation. Keap1$^{+/+}$ (n=20); Keap1$^{R554Q/+}$ (n=11); Keap1$^{R554Q/R554Q}$ (n=25). **(B)** Overall
539 survival of Kras$^{G12D/+}$; p53$^{fl/fl}$ mice with Nrf2 mutation. Nrf2$^{+/+}$ (n=25); Nrf2$^{D29H/+}$ (n=29).
540 Ns = not significant (Log-rank (Mantel-Cox) test). **(C)** Representative
541 immunohistochemical (IHC) staining of Nrf2 in Kras$^{G12D/+}$; p53$^{fl/fl}$ mice with Keap1/Nrf2
542 mutation (scale bars = 20 μM). **(D)** H-scores for Nrf2 (nuclear) IHC staining. **(E)**
543 Representative immunohistochemical (IHC) staining of Nrf2 target Nqo1 (scale bars =
544 20 μM). **(F)** H-scores for Nqo1 (whole cell) IHC staining. For **C-F**, N=3 mice per
545 genotype and >20,000 tumor cells per mouse. *p<0.05 (one-way ANOVA). **(G)**
546 Representative whole lung H&E stained section (scale bars = 2000 μM). **(H)** Distribution
547 of tumor grades across Keap1/Nrf2 mutant models. *p<0.05 (unpaired t test with Holm-
548 Sidak's multiple comparisons test). $ = fewer than 3 tumors detected across all mice. **(I)**
549 Fraction of lung tumor burden by grade (lung tumor area per grade/ total lung area).
550 *p<0.05 (unpaired t test with Holm-Sidak's multiple comparisons test). $ = fewer than 3
551 tumors detected across all mice. For both **(H)** and **(I)** n≥9 mice and ≥1,900 tumors per
552 genotype. Only one grade 5 tumor was found in the Keap1$^{R554Q/R554Q}$ cohort, and
553 therefore was excluded from these analyses.

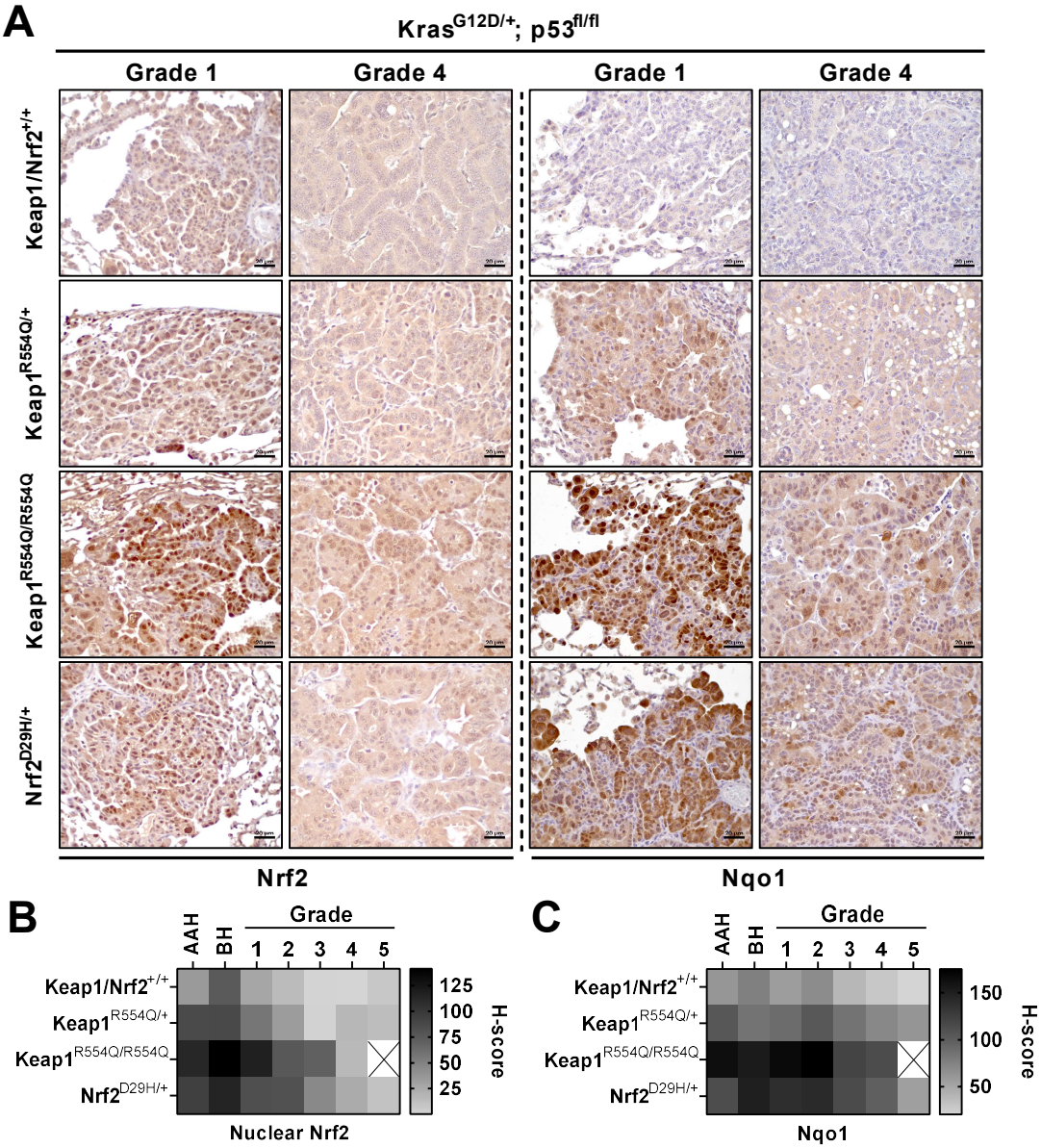
A
Kras$^{G12D/+}$; p53$^{fl/fl}$
Grade 1
Grade 4
Grade 1
Grade 4
Keap1/Nrf2$^{+/+}$
Keap1$^{R554Q/+}$
Keap1$^{R554Q/R554Q}$
Nrf2$^{D29H/+}$
Nrf2
Nqo1
B
AAH
BH
Grade
1 2 3 4 5
Keap1/Nrf2$^{+/+}$
Keap1$^{R554Q/+}$
Keap1$^{R554Q/R554Q}$
Nrf2$^{D29H/+}$
125
100
75
50
25
H-score
Nuclear Nrf2
C
AAH
BH
Grade
1 2 3 4 5
Keap1/Nrf2$^{+/+}$
Keap1$^{R554Q/+}$
Keap1$^{R554Q/R554Q}$
Nrf2$^{D29H/+}$
150
100
50
H-score
Nqo1

554 **Figure 6. Nrf2 expression and activity is reduced in higher-grade tumors. (A)**
555 Representative Nrf2 and Nqo1 IHC staining in grade 1 and 4 tumors from $Kras^{G12D/+}$;
556 $p53^{fl/fl}$ mice with Keap1 or Nrf2 mutation (scale bars = 20 μM). **(B, C)** Heatmaps
557 depicting the H-scores per grade from IHC staining for Nrf2 (nuclear) **(B)** and the Nrf2
558 target Nqo1 (whole cell) **(C)**. N=3 mice per genotype, >20,000 tumor cells per mouse.
559 Only one grade 5 tumor was found in the $Keap1^{R554Q/R554Q}$ cohort, and therefore was
560 excluded from these analyses.

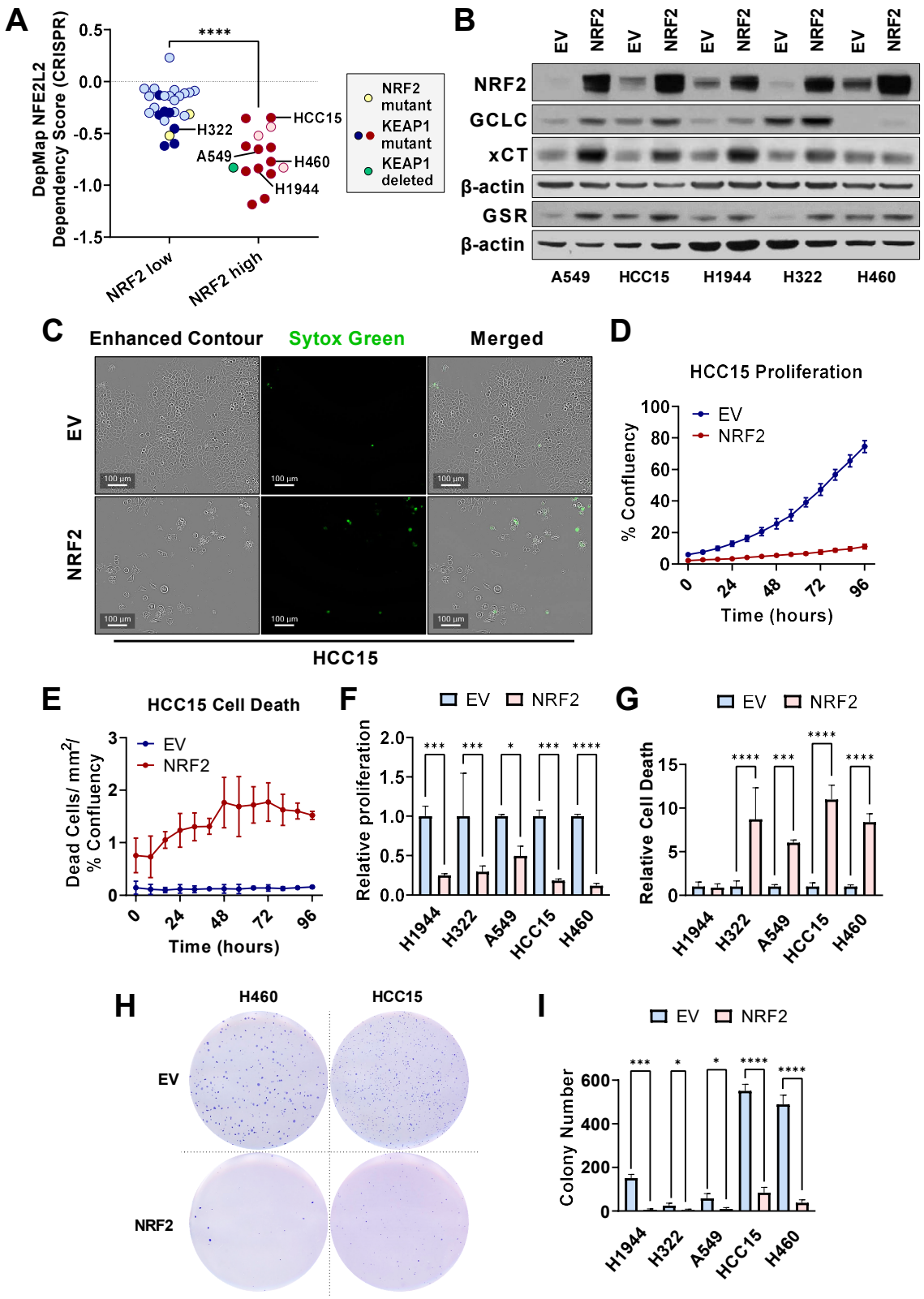
A
DepMap NFE2L2 Dependency Score (CRISPR)
****
HCC15
H322
A549
H460
H1944
NRF2 low
NRF2 high
NRF2 mutant
KEAP1 mutant
KEAP1 deleted
B
EV
NRF2
NRF2
GCLC
xCT
β-actin
GSR
β-actin
A549
HCC15
H1944
H322
H460
C
Enhanced Contour
Sytox Green
Merged
EV
NRF2
HCC15
D
HCC15 Proliferation
% Confluency
Time (hours)
E
HCC15 Cell Death
Dead Cells/ mm²/ % Confluency
Time (hours)
F
Relative proliferation
G
Relative Cell Death
H
H460
HCC15
EV
NRF2
I
Colony Number

561 **Figure 7. NRF2 overexpression impairs lung cancer cell proliferation, viability,**
562 **and soft agar colony formation. (A)** Dependency scores obtained from DepMap[52] and
563 represented as *NFEL2* 22Q2 Public+Score, Chronos for NSCLC cell lines previously
564 determined to have high or low NRF2 activity[22]. NRF2 mutant line symbols are
565 represented by yellow, KEAP1 mutant lines by dark red or dark blue, and KEAP1
566 deleted lines by green. ***$p<0.0001$ (unpaired t-test). **(B)** Western blot analysis of
567 NRF2, β-actin, and NRF2 target GCLC, xCT, and GSR expression in *KEAP1* mutant
568 lung cancer cell lines transduced with PLX317-empty vector (EV) or PLX317-NRF2
569 (NRF2). **(C)** Representative images of HCC15 cells transduced with EV or NRF2
570 demonstrating cell confluency (enhanced contour) and cell death (Sytox Green) (scale
571 bars = 100 μM). **(D, E)** Analysis of EV and NRF2 HCC15 cell proliferation and death
572 over 96 hours. Proliferation is represented as % confluency at each time point, and cell
573 death as the number of Sytox Green positive cells per area normalized to % confluency.
574 N=3 technical replicates per cell line, and two independent experiments. **(F, G)** Area
575 under the curve (AUC) analysis of cell proliferation **(F)** and Sytox Green-positive cell
576 death **(G)** in KEAP1 mutant lung cancer cells lines +/- NRF2, normalized to empty
577 vector control. *$p<0.05$ (one-way ANOVA). For **(C-G)** NSCLC cells were seeded in
578 triplicate in 96-well plates at a density of 2,500 cells/ well. **(H)** Representative images of
579 H460 and HCC15 soft agar colony formation +/- NRF2. **(I)** Quantification of soft agar
580 colony number of *KEAP1* mutant lung cancer cell lines. *$p<0.05$ (one-way ANOVA).
581 N=3 technical replicates per cell line, two independent experiments. For **(H, I),** 5,000
582 cells per well were seeded in 6-well plates in triplicate.

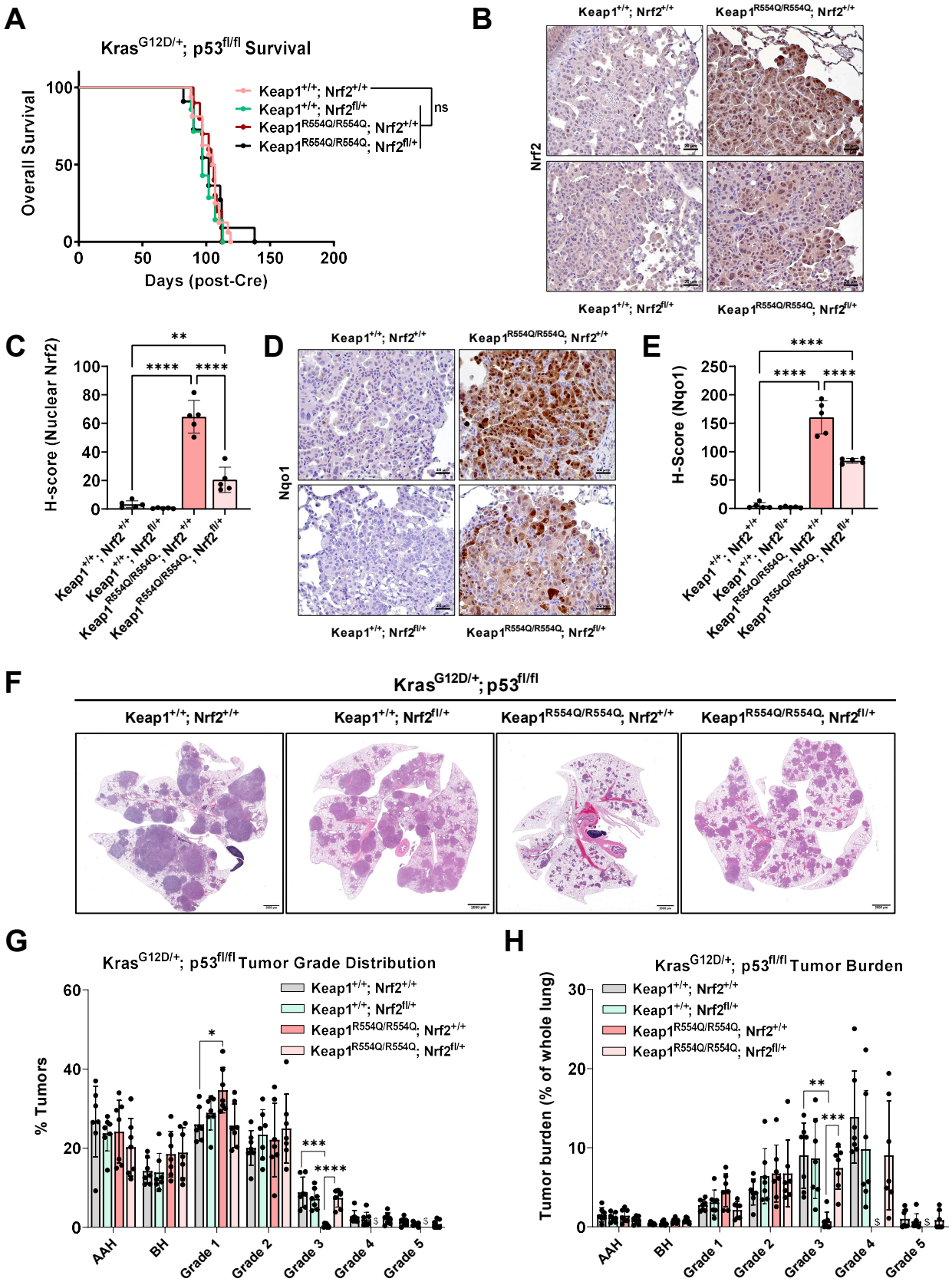
A
Kras$^{G12D/+}$; p53$^{fl/fl}$ Survival
Overall Survival
Days (post-Cre)
Keap1$^{+/+}$; Nrf2$^{+/+}$
Keap1$^{+/+}$; Nrf2$^{fl/+}$
Keap1$^{R554Q/R554Q}$; Nrf2$^{+/+}$
Keap1$^{R554Q/R554Q}$; Nrf2$^{fl/+}$
ns
B
Nrf2
C
H-score (Nuclear Nrf2)
D
Nqo1
E
H-Score (Nqo1)
F
Kras$^{G12D/+}$; p53$^{fl/fl}$
G
Kras$^{G12D/+}$; p53$^{fl/fl}$ Tumor Grade Distribution
% Tumors
AAH
BH
Grade 1
Grade 2
Grade 3
Grade 4
Grade 5
H
Kras$^{G12D/+}$; p53$^{fl/fl}$ Tumor Burden
Tumor burden (% of whole lung)

583 **Figure 8. Single copy Nrf2 deletion rescues homozygous Keap1^{R554Q}-mediated**
584 **adenocarcinoma progression impairment in the Kras$^{G12D/+}$; p53$^{fl/fl}$ model. (A)**
585 Overall survival of Kras$^{G12D/+}$; p53$^{fl/fl}$ mice with Keap1 mutation and/ or single copy Nrf2
586 deletion. Keap1$^{+/+}$; Nrf2$^{+/+}$ (n=16), Keap1$^{+/+}$; Nrf2$^{fl/+}$ (n=7), Keap1$^{R554Q/R554Q}$; Nrf2$^{+/+}$
587 (n=10), Keap1$^{R554Q/R554Q}$; Nrf2$^{fl/+}$ (n=11). Ns = not significant (Log-rank (Mantel-Cox)
588 test). **(B)** Representative immunohistochemical (IHC) staining of Nrf2 in Kras$^{G12D/+}$;
589 p53$^{fl/fl}$ mice with Keap1 mutation and/ or heterozygous Nrf2 deletion (scale bars = 20
590 μM). **(C)** H-scores for Nrf2 (nuclear) IHC staining. **(D)** Representative IHC staining of
591 Nrf2 target Nqo1 (scale bars = 20 μM). **(E)** H-scores for Nqo1 (whole-cell) IHC staining.
592 For **B-E**, N=3 mice per genotype and >20,000 tumor cells per mouse. *$p<0.05$ (one-way
593 ANOVA). **(F)** Representative whole lung H&E-stained sections (scale bars = 2000 μM).
594 **(G)** Distribution of tumor grades across Keap1 mutant/ Nrf2-deleted models. *$p<0.05$
595 (unpaired t test with Holm-Sidak's multiple comparisons test). $ = fewer than 3 tumors
596 detected across all mice. **(H)** Fraction of lung tumor burden by grade (lung tumor area
597 per grade/ total lung area). *$p<0.05$ (unpaired t test with Holm-Sidak's multiple
598 comparisons test). $ = fewer than 3 tumors detected across all mice. For both **(G)** and
599 **(H)** n=7 mice and $\geq$1,000 tumors per genotype were analyzed. Only one grade 4 and
600 one grade 5 tumor were found in the Keap1$^{R554Q/R554Q}$ cohort, and therefore were
601 excluded from these analyses.

602 **References**

603 1 DeBlasi, J. M. & DeNicola, G. M. Dissecting the Crosstalk between NRF2
604 Signaling and Metabolic Processes in Cancer. *Cancers (Basel)* **12**,
605 doi:10.3390/cancers12103023 (2020).
606 2 He, F., Ru, X. & Wen, T. NRF2, a Transcription Factor for Stress Response and
607 Beyond. *Int J Mol Sci* **21**, doi:10.3390/ijms21134777 (2020).
608 3 Itoh, K. *et al.* Keap1 represses nuclear activation of antioxidant responsive
609 elements by Nrf2 through binding to the amino-terminal Neh2 domain. *Genes*
610 *Dev* **13**, 76-86, doi:10.1101/gad.13.1.76 (1999).
611 4 Ramos-Gomez, M., Dolan, P. M., Itoh, K., Yamamoto, M. & Kensler, T. W.
612 Interactive effects of nrf2 genotype and oltipraz on benzo[a]pyrene–DNA
613 adducts and tumor yield in mice. *Carcinogenesis* **24**, 461-467,
614 doi:10.1093/carcin/24.3.461 (2003).
615 5 Ramos-Gomez, M. *et al.* Sensitivity to carcinogenesis is increased and
616 chemoprotective efficacy of enzyme inducers is lost in nrf2 transcription
617 factor-deficient mice. *Proceedings of the National Academy of Sciences* **98**,
618 3410-3415, doi:doi:10.1073/pnas.051618798 (2001).
619 6 Aoki, Y. *et al.* Accelerated DNA adduct formation in the lung of the Nrf2 knockout
620 mouse exposed to diesel exhaust. *Toxicol Appl Pharmacol* **173**, 154-160,
621 doi:10.1006/taap.2001.9176 (2001).
622 7 Iida, K. *et al.* Nrf2 Is Essential for the Chemopreventive Efficacy of Oltipraz
623 against Urinary Bladder Carcinogenesis. *Cancer Research* **64**, 6424-6431,
624 doi:10.1158/0008-5472.Can-04-1906 (2004).
625 8 Kensler, T. W. & Wakabayashi, N. Nrf2: friend or foe for chemoprevention?
626 *Carcinogenesis* **31**, 90-99, doi:10.1093/carcin/bgp231 (2010).
627 9 Schmidlin, C. J., Shakya, A., Dodson, M., Chapman, E. & Zhang, D. D. The
628 intricacies of NRF2 regulation in cancer. *Semin Cancer Biol* **76**, 110-119,
629 doi:10.1016/j.semcancer.2021.05.016 (2021).
630 10 Telkoparan-Akillilar, P., Suzen, S. & Saso, L. Pharmacological Applications of
631 Nrf2 Inhibitors as Potential Antineoplastic Drugs. *Int J Mol Sci* **20**,
632 doi:10.3390/ijms20082025 (2019).
633 11 Network, C. G. A. R. Comprehensive molecular profiling of lung adenocarcinoma.
634 *Nature* **511**, 543-550, doi:10.1038/nature13385 (2014).
635 12 Network, C. G. A. R. Comprehensive genomic characterization of squamous cell
636 lung cancers. *Nature* **489**, 519-525, doi:10.1038/nature11404 (2012).
637 13 Singh, A. *et al.* Dysfunctional KEAP1-NRF2 interaction in non-small-cell lung
638 cancer. *PLoS Med* **3**, e420, doi:10.1371/journal.pmed.0030420 (2006).
639 14 Shibata, T. *et al.* Cancer related mutations in NRF2 impair its recognition by
640 Keap1-Cul3 E3 ligase and promote malignancy. *Proc Natl Acad Sci U S A* **105**,
641 13568-13573, doi:10.1073/pnas.0806268105 (2008).
642 15 Wang, R. *et al.* Hypermethylation of the Keap1 gene in human lung cancer cell
643 lines and lung cancer tissues. *Biochem Biophys Res Commun* **373**, 151-154,
644 doi:10.1016/j.bbrc.2008.06.004 (2008).
645 16 Kim, Y. R. *et al.* Oncogenic NRF2 mutations in squamous cell carcinomas of
646 oesophagus and skin. *J Pathol* **220**, 446-451, doi:10.1002/path.2653 (2010).

17 Zhang, P. *et al.* Loss of Kelch-like ECH-associated protein 1 function in prostate cancer cells causes chemoresistance and radioresistance and promotes tumor growth. *Mol Cancer Ther* **9**, 336-346, doi:10.1158/1535-7163.MCT-09-0589 (2010).
18 Solis, L. M. *et al.* Nrf2 and Keap1 abnormalities in non-small cell lung carcinoma and association with clinicopathologic features. *Clin Cancer Res* **16**, 3743-3753, doi:10.1158/1078-0432.CCR-09-3352 (2010).
19 Sporn, M. B. & Liby, K. T. NRF2 and cancer: the good, the bad and the importance of context. *Nat Rev Cancer* **12**, 564-571, doi:10.1038/nrc3278 (2012).
20 Singh, A., Bodas, M., Wakabayashi, N., Bunz, F. & Biswal, S. Gain of Nrf2 function in non-small-cell lung cancer cells confers radioresistance. *Antioxidants and Redox Signaling*, doi:10.1089/ars.2010.3219 (2010).
21 Denicola, G. M. *et al.* Oncogene-induced Nrf2 transcription promotes ROS detoxification and tumorigenesis. *Nature* **475**, 106-110, doi:10.1038/nature10189 (2011).
22 DeNicola, G. M. *et al.* NRF2 regulates serine biosynthesis in non-small cell lung cancer. *Nature Genetics* **47**, 1475-1481, doi:10.1038/ng.3421 (2015).
23 Mitsuishi, Y. *et al.* Nrf2 redirects glucose and glutamine into anabolic pathways in metabolic reprogramming. *Cancer Cell* **22**, 66-79, doi:10.1016/j.ccr.2012.05.016 (2012).
24 Sayin, V. I. *et al.* Activation of the NRF2 antioxidant program generates an imbalance in central carbon metabolism in cancer. *Elife* **6**, doi:10.7554/eLife.28083 (2017).
25 Lignitto, L. *et al.* Nrf2 Activation Promotes Lung Cancer Metastasis by Inhibiting the Degradation of Bach1. *Cell* **178**, 316-329.e318, doi:10.1016/j.cell.2019.06.003 (2019).
26 Best, S. A. *et al.* Synergy between the KEAP1/NRF2 and PI3K Pathways Drives Non-Small-Cell Lung Cancer with an Altered Immune Microenvironment. *Cell Metabolism* **27**, 935-943.e934, doi:10.1016/j.cmet.2018.02.006 (2018).
27 Best, S. A. *et al.* Distinct initiating events underpin the immune and metabolic heterogeneity of KRAS-mutant lung adenocarcinoma. *Nature Communications* **10**, 1-14, doi:10.1038/s41467-019-12164-y (2019).
28 Hayashi, M. *et al.* Microenvironmental Activation of Nrf2 Restricts the Progression of Nrf2-Activated Malignant Tumors. *Cancer Res* **80**, 3331-3344, doi:10.1158/0008-5472.Can-19-2888 (2020).
29 Jeong, Y. *et al.* Role of KEAP1/NRF2 and TP53 mutations in lung squamous cell carcinoma development and radiation resistance. *Cancer Discovery* **7**, 86-101, doi:10.1158/2159-8290.CD-16-0127 (2017).
30 Kang, Y. P. *et al.* Cysteine dioxygenase 1 is a metabolic liability for non-small cell lung cancer. *eLife*, doi:10.7554/eLife.45572 (2019).
31 Romero, R. *et al.* Keap1 mutation renders lung adenocarcinomas dependent on Slc33a1. *Nature Cancer* **1**, 589-602, doi:10.1038/s43018-020-0071-1 (2020).
32 Romero, R. *et al.* Keap1 loss promotes Kras-driven lung cancer and results in dependence on glutaminolysis. *Nature Medicine*, doi:10.1038/nm.4407 (2017).

691 33 Singh, A. *et al.* NRF2 Activation Promotes Aggressive Lung Cancer and
692 Associates with Poor Clinical Outcomes. *Clinical Cancer Research* **27**, 877,
693 doi:10.1158/1078-0432.CCR-20-1985 (2021).
694 34 Foggetti, G. *et al.* Genetic Determinants of EGFR-Driven Lung Cancer Growth
695 and Therapeutic Response In Vivo. *Cancer Discovery* **11**, 1736-1753,
696 doi:10.1158/2159-8290.Cd-20-1385 (2021).
697 35 Rogers, Z. N. *et al.* Mapping the in vivo fitness landscape of lung
698 adenocarcinoma tumor suppression in mice. *Nature Genetics*,
699 doi:10.1038/s41588-018-0083-2 (2018).
700 36 Cai, H. *et al.* A Functional Taxonomy of Tumor Suppression in Oncogenic KRAS-
701 Driven Lung Cancer. *Cancer Discov* **11**, 1754-1773, doi:10.1158/2159-8290.Cd-
702 20-1325 (2021).
703 37 Rogers, Z. N. *et al.* A quantitative and multiplexed approach to uncover the
704 fitness landscape of tumor suppression in vivo. *Nature Methods* **14**, 737-742,
705 doi:10.1038/nmeth.4297 (2017).
706 38 Hast, B. E. *et al.* Cancer-derived mutations in KEAP1 impair NRF2 degradation
707 but not ubiquitination. *Cancer Research*, doi:10.1158/0008-5472.CAN-13-1655
708 (2014).
709 39 Tong, K. I. *et al.* Different Electrostatic Potentials Define ETGE and DLG Motifs
710 as Hinge and Latch in Oxidative Stress Response. *Molecular and Cellular*
711 *Biology*, doi:10.1128/mcb.00753-07 (2007).
712 40 Taguchi, K. *et al.* Genetic Analysis of Cytoprotective Functions Supported by
713 Graded Expression of Keap1. *Molecular and Cellular Biology*,
714 doi:10.1128/mcb.01591-09 (2010).
715 41 Wakabayashi, N. *et al.* Keap1-null mutation leads to postnatal lethality due to
716 constitutive Nrf2 activation. *Nature Genetics*, doi:10.1038/ng1248 (2003).
717 42 Huppke, P. *et al.* Activating de novo mutations in NFE2L2 encoding NRF2 cause
718 a multisystem disorder. *Nature Communications* **8**, 818, doi:10.1038/s41467-
719 017-00932-7 (2017).
720 43 Jackson, E. L. *et al.* Analysis of lung tumor initiation and progression using
721 conditional expression of oncogenic K-ras. *Genes and Development*,
722 doi:10.1101/gad.943001 (2001).
723 44 Jackson, E. L. *et al.* The differential effects of mutant p53 alleles on advanced
724 murine lung cancer. *Cancer Research* **65**, 10280-10288, doi:10.1158/0008-
725 5472.CAN-05-2193 (2005).
726 45 Lo, S. C. & Hannink, M. PGAM5 tethers a ternary complex containing Keap1 and
727 Nrf2 to mitochondria. *Exp Cell Res* **314**, 1789-1803,
728 doi:10.1016/j.yexcr.2008.02.014 (2008).
729 46 Ma, J. *et al.* PALB2 interacts with KEAP1 to promote NRF2 nuclear accumulation
730 and function. *Mol Cell Biol* **32**, 1506-1517, doi:10.1128/MCB.06271-11 (2012).
731 47 Mulvaney, K. M. *et al.* Identification and characterization of MCM3 as a kelch-like
732 ECH-associated protein 1 (KEAP1) substrate. *Journal of Biological Chemistry*
733 **291**, 23719-23733, doi:10.1074/jbc.M116.729418 (2016).
734 48 Marzio, A. *et al.* EMSY inhibits homologous recombination repair and the
735 interferon response, promoting lung cancer immune evasion. *Cell* **185**, 169-
736 183.e119, doi:10.1016/j.cell.2021.12.005 (2022).

49 Zhang, Y. *et al.* Emerging Substrate Proteins of Kelch-like ECH Associated Protein 1 (Keap1) and Potential Challenges for the Development of Small-Molecule Inhibitors of the Keap1-Nuclear Factor Erythroid 2-Related Factor 2 (Nrf2) Protein–Protein Interaction. *Journal of Medicinal Chemistry* **1**, doi:10.1021/acs.jmedchem.9b01865 (2020).
50 McCutcheon, D. C., Lee, G., Carlos, A., Montgomery, J. E. & Moellering, R. E. Photoproximity Profiling of Protein-Protein Interactions in Cells. *J Am Chem Soc* **142**, 146-153, doi:10.1021/jacs.9b06528 (2020).
51 Kitamura, H. & Motohashi, H. NRF2 addiction in cancer cells. *Cancer Sci* **109**, 900-911, doi:10.1111/cas.13537 (2018).
52 Institute, B. DepMap Public 22Q2 (2022).
53 Hamad, S. H. *et al.* TP53, CDKN2A/P16, and NFE2L2/NRF2 regulate the incidence of pure- and combined-small cell lung cancer in mice. *Oncogene* **41**, 3423-3432, doi:10.1038/s41388-022-02348-0 (2022).
54 Tuveson, D. A. *et al.* Endogenous oncogenic K-ras(G12D) stimulates proliferation and widespread neoplastic and developmental defects. *Cancer Cell* **5**, 375-387, doi:10.1016/s1535-6108(04)00085-6 (2004).
55 Murphy, D. J. *et al.* Distinct thresholds govern Myc's biological output in vivo. *Cancer Cell* **14**, 447-457, doi:10.1016/j.ccr.2008.10.018 (2008).
56 Jamal-Hanjani, M. *et al.* Tracking the Evolution of Non–Small-Cell Lung Cancer. *New England Journal of Medicine* **376**, 2109-2121, doi:10.1056/NEJMoa1616288 (2017).
57 McLoughlin, M. R. *et al.* TrxR1, Gsr, and oxidative stress determine hepatocellular carcinoma malignancy. *Proc Natl Acad Sci U S A* **116**, 11408-11417, doi:10.1073/pnas.1903244116 (2019).
58 Bankhead, P. *et al.* QuPath: Open source software for digital pathology image analysis. *Sci Rep* **7**, 16878, doi:10.1038/s41598-017-17204-5 (2017).
59 Berger, A. H. *et al.* High-throughput Phenotyping of Lung Cancer Somatic Mutations. *Cancer Cell* **30**, 214-228, doi:10.1016/j.ccell.2016.06.022 (2016).